Journal of Alloys and Compounds 509 (2011) 4967–4971

Contents lists available at ScienceDirect

Journal of Alloys and Compounds

journal homepage: www.elsevier.com/locate/jallcom

Impedance spectroscopy and dielectric properties of Ce and La substituted $Pb_{0.7}Sr_{0.3}(Fe_{0.012}Ti_{0.988})O_3$ nanoparticles

Kuldeep Chand Verma [a,*], Mast Ram [b], Jitender Singh [a], R.K. Kotnala [c]

[a] Department of Physics, Eternal University, Baru Sahib, HP 173101, India
[b] Department of Physics, Himachal Pradesh University, Shimla, HP 171005, India
[c] National Physical Laboratory, New Delhi 110012, India

ARTICLE INFO

Article history:
Received 18 May 2010
Received in revised form 9 January 2011
Accepted 21 January 2011
Available online 2 February 2011

Keywords:
Multiferroics
Chemical synthesis
Dielectric response
Impedance spectroscopy
Grain boundaries

ABSTRACT

We present the structural, microstructural, dielectric and impedance behavior of $Pb_{0.7}Sr_{0.3}[(Fe_{2/3}Ce_{1/3})_{0.012}Ti_{0.988}]O_3$ (PSFCT) and $Pb_{0.7}Sr_{0.3}[(Fe_{2/3}La_{1/3})_{0.012}Ti_{0.988}]O_3$ (PSFLT) nanoparticles. These nanoparticles were prepared by a chemical synthesis route using polyvinyl alcohol as surfactant. The X-ray diffraction pattern shows polycrystalline nature with coexistence of tetragonal and cubic phase in both PSFCT and PSFLT nanoparticles. The average particle size has been measured using Scherer's relation. The average particle sizes also measured by TEM are 10 and 11 nm, and by SEM 9 and 12 nm, respectively, of PSFCT and PSFLT nanoparticles. By measuring the value of relative permittivity (ε') and loss ($\tan\delta$) at lower frequency, the dielectric properties show Maxwell–Wagner type interfacial polarization. However, due to nano size effect of PSFCT and PSFLT, dispersionless dielectric response has been observed up to higher frequency of 15 MHz. The frequency dependent real (Z') and imaginary (Z'') parts of impedance confirmed the variation which was observed in dielectric properties. The values of resistance of grain boundaries, R_{gb} is higher than grains, R_g indicates that the effect of grain boundaries is dominant on electrical properties when the size of nanoparticles is quite small.

1. Introduction

Recently, multiferroics (MF) with perovskite structure (ABO_3) have been extensively studied due to the diversity of their physical properties. Perovskite $PbTiO_3$ based MF are substituted with different elements such as transition metal ions (M = Fe, Ni, Co, etc.) [1,2] or with rare earth metal ions (M = Ce, La, W, etc.) [3,4], making a heterostructure, i.e., $CoFe_2O_4/Pb(Zr_{0.53}Ti_{0.47})O_3$ [5], $La_{0.6}Sr_{0.4}MnO_3/0.7Pb(Mg_{1/3}Nb_{2/3})O_3$ $0.3PbTiO_3$ [6] and MF composites. In addition to the coexistence of ferroelectricity and ferromagnetism, the magnetoelectric (ME) coupling (i.e., magnetic degree of freedom can be manipulated by an electric field and vice versa) for spintronic devices [1–6], and the occurrence of good dielectric properties for various applications (i.e., tunable mixers, phase shifters, voltage controlled oscillators, delay lines and ultra large-scale integration dynamic random access memory (DRAM) capacitors) of MF are highly important [7,8]. The dielectric properties of nanostructured MF and ferroelectrics are suitable for those devices which operate at higher frequencies [7,9]. The dielectric properties are dependent on several factors, such as method of preparation, heat treatment, sintering conditions, chemical composition, cation distribution and crystallite size.

The impedance spectroscopy (IS) is a very convenient and powerful experimental technique that enables us to correlate the dielectric properties of a material with its microstructure and helps to analyze and separate the contributions from various components (i.e., through grains, grain boundary, interfaces, etc.) of polycrystalline materials over wide frequency range. The technique also allows the measurement of capacitance (C) and the loss tangent ($\tan\delta$) and real and imaginary impedance with varying frequency range. From the measured capacitance and $\tan\delta$, four complex dielectric parameters can be computed—impedance (Z^*), permittivity (ε^*), electric modulus (M^*) and admittance (Y^*). If the current I and voltage V are considered to have time variation of $e^{i\omega t}$, the quantity V/I is a complex number with no time dependence and is called the complex impedance Z^*. The real part (Z') is interpreted as resistance and the imaginary part (Z'') is interpreted as capacitance with $Z^{-1} = 1/R + j\omega C$ where $j = \sqrt{-1}$, C is the capacitance and ω is the angular frequency of the *ac* field. In general, the values of resistance (R) and capacitance (C) of a perfect crystal can be analyzed by an equivalent circuit combination of parallel resistance–capacitance (RC) called Nyquist diagram. This RC circuit gives rise to one semicircular arc on the complex plane, which intercepts the Z' axis at zero and R. For a bulk crystal containing interfacial layers, the equivalent circuit may be considered as two parallel RC circuit connected

* Corresponding author. Tel.: +91 9418941286; fax: +91 0177 2830775.
E-mail addresses: kuldeep0309@yahoo.co.in (K.C. Verma), mastram1999@yahoo.com (M. Ram).

0925-8388/$ – see front matter © 2011 Elsevier B.V. All rights reserved.
doi:10.1016/j.jallcom.2011.01.144

in serial, giving rise to two arcs in complex plane: one for grain and the other for grain boundary. The arc of bulk generally lies at the frequency range higher than that of grain boundary [10–12]. The high-frequency semicircular arc can be attributed to the contributions from the bulk materials, arising due to a parallel combination of bulk resistance and bulk capacitance. The low frequency semicircular arc can be attributed to the contributions of grain boundary, arising due to a parallel combination of grain boundary resistance and capacitance. Besides the two semicircular arcs of grains and grain boundary, a very small semicircular arc also exists in some cases at sufficiently lower frequency; this may be due to the contribution of interfaces.

Recently, Verma et al. reported the dielectric properties of nano MF systems of $(Pb)(Fe,Ti)O_3$ (PFT) [13] and Sr substituted PFT (PSFT) [14] based on perovskite $PbTiO_3$. Due to the presence of two unpaired electrons in 6*p* orbital of Pb^{2+}, there is small off-centering displacement of Fe^{3+} and Ti^{4+} ions which gives less polarization. In this paper, we report enhancement in dielectric properties of MF PSFT by substituting Ce and La with Fe. The free electrons in $4f^2$ orbital of Ce^{3+} and $5d^1$ of La^{3+} are responsible for pairing 6*p* orbital of Pb^{2+} and giving one more lone pair of electron along A-site. As a result, a large off-centering displacement (d^0) is possible that increases the value of polarization. The large electronegativity differences of dopant Ce^{3+} and La^{3+} with Pb^{2+}, Fe^{3+} and Ti^{4+} ions increase the bond length between atoms inside the unit cell which leads to stretching of bonds and thus results in large polarization [15].

Here, we present the improvement in dielectric properties of $Pb_{0.7}Sr_{0.3}[(Fe_{2/3}Ce_{1/3})_{0.012}Ti_{0.988}]O_3$ (PSFCT) and $Pb_{0.7}Sr_{0.3}[(Fe_{2/3}La_{1/3})_{0.012}Ti_{0.988}]O_3$ (PSFLT), nanomultiferroics. The IS measurements have been used to study the effect of grains, grain boundaries, interfaces, etc. on dielectric properties at lower and higher frequency regions.

2. Experimental

2.1. Synthesis

The PSFCT and PSFLT nanoparticles were prepared by a chemical synthesis route using polyvinyl alcohol (PVA) as surfactant. The PSFCT/PSFLT precursor was prepared from lead acetate, strontium acetate, ferric chloride, cerium chloride, lanthanum nitrate and tetra-n-butyl orthotitanate were dissolved in acetic acid, ethyl alcohol and distilled water. The detailed procedure for synthesis is described elsewhere [2,13]. These PSFCT and PSFLT precursor powders were then heated at 700 °C/2 h for crystallization. The phase structure was analyzed by X-ray diffraction (XRD) using X-Pert PRO system and microstructure by transmission/scanning electron microscopy (TEM/SEM) (Hitachi H-7500/JEOL JSM6100). For electrical measurements, PSFCT and PSFLT heated powder were pressed into pellet form using a pressure of 5 bars for 10 min and then sintered at higher temperature of ~1000 °C for 5 h.

2.2. X-ray diffraction studies

The heated powder was characterized for their phase purity and crystallinity by powder X-ray diffraction measurements with CuKα radiation at room temperature. The average crystallite size of the particles was determined by using the Debye–Scherer formula (1):

$$D = \frac{0.9\lambda}{\beta \cos\theta} \tag{1}$$

here λ = wavelength of the CuKα radiation (λ = 1.54 Å), β = full width half maximum (FWHM) in radians calculated using Gaussian fitting. The contribution due to broadening of XRD peaks has been taken into account in order to obtain the accurate crystallite size.

The X-ray density of prepared specimens was calculated using the relation

$$d_x = \frac{ZM}{Na^3} \tag{2}$$

where *Z* is the number of molecules per unit cell, *M* is the molecular weight, *a* is the lattice parameter and *N* is the Avogadro's number. The apparent density (experimental) is calculated by assuming the cylindrical shape of the pellets and using the relation (3):

$$d_a = \frac{m}{V} = \frac{m}{\pi r^2 h} \tag{3}$$

here *m*, *V*, *r*, *h* are mass, volume, radius and thickness of the specimen, respectively. The percentage porosity was calculated using relation:

$$P = 1 - \frac{d_a}{d_x} \tag{4}$$

2.3. Electrical measurements

The capacitance, dielectric and IS measurements were carried out on pellet specimen (sintered at 1000 °C) in the frequency range 20 Hz to 20 MHz by using Precision Impedance analyzer (Wayne Kerr 6500B).

The value of dielectric constant was calculated using the relation (5)

$$\varepsilon' = \frac{C_p d}{\varepsilon_o A} \tag{5}$$

where ε_o is the permittivity of free space, *d* is the thickness, *A* is the area of cross-section and C_p is the measured value of the capacitance of the pellet.

The complex dielectric constant (ε^*) and loss tangent ($\tan\delta$) of the specimens are calculated using the following relation (6) and (7):

$$\varepsilon^* = \varepsilon' - j\varepsilon'' = \varepsilon' \tan\delta \tag{6}$$

and

$$\tan\delta = \frac{1}{2\pi f \varepsilon_o \varepsilon' \rho} \tag{7}$$

where $\tan\delta$ is the dielectric loss which gives the loss of energy from the applied field into the specimen and is therefore denoted as the dielectric loss, *f* is the frequency of the applied field and ρ is the resistivity.

2.4. Impedance studies

The impedance can be represented ideally by an equivalent circuit consisting of two parallel *RC* elements in series as discussed in Section 1. This circuit can be used to interpret the electrical regions within materials whose properties are separated in terms of contribution from grains (bulk) and grain boundary impedances connected in series [11,12].

3. Results and discussion

3.1. XRD, density and microstructure characterization

Fig. 1 shows the XRD pattern of PSFCT and PSFLT nanoparticles heated with 700 °C/2 h. The XRD data shows polycrystalline nature of both the specimens with one peak of pyrochlore phase exists only in PSFLT. The reflection lines (0 0 1), (1 0 0), (1 0 1), (1 1 0), (1 1 1), (0 0 2), (2 0 0) and (1 0 2) are observed at diffraction angle $2\theta = 21.43°, 22.77°, 31.45°, 32.41°, 39.18°, 43.62°, 46.51°$ and 50.17°, respectively, which are matched well with the ASTM card for tetragonal structure of parent perovskite $PbTiO_3$. The values of lattice parameters are $a = 3.924$ Å, $c = 3.935$ Å and $c/a = 1.0028$ for PSFCT, and $a = 3.923$ Å, $c = 3.936$ Å and $c/a = 1.0033$ for PSFLT nanoparticles. These distortion ratios (c/a) are very small as compared with the parent $PbTiO_3$ (1.066). Such a significant reduction exists due to the substitution of Sr, Fe, Ce and La in perovskite $PbTiO_3$. Because these substituted ions have large variations in ionic radii, i.e., Sr^{2+} (1.32 Å), Fe^{3+} (0.63 Å), Ce^{3+} (1.15 Å) and La^{3+} (1.17 Å), with parent $PbTiO_3$ (Pb^{2+} (1.33 Å) and Ti^{3+} (0.81 Å). The small distortions (c/a values) indicate the possibility of the coexistence of both tetragonal and cubic phases in the specimens. The average particle's size using Scherer's relation is 11 nm for PSFCT and 12 nm for PSFLT nanoparticles. These formation of small nano particles exist because of the use of PVA as surfactant in the present chemical route. PVA serves as surfactant to encapsulate the cationic species in divided groups during the reaction. Therefore, a controlled reaction occurs that confine the size and morphology of the specimen.

The variation of the X-ray density (theoretical density) and apparent density (experimental density) with Sr^{2+}, Fe^{3+}, Ce^{3+}, La^{3+} and Ti^{4+} ions in perovskite $PbTiO_3$ has been calculated by using Eqs. (2) and (3). The values of theoretical density are 8.39 and 8.43 g cm^{-3}, and apparent densities are 8.27 and 8.23 g cm^{-3},

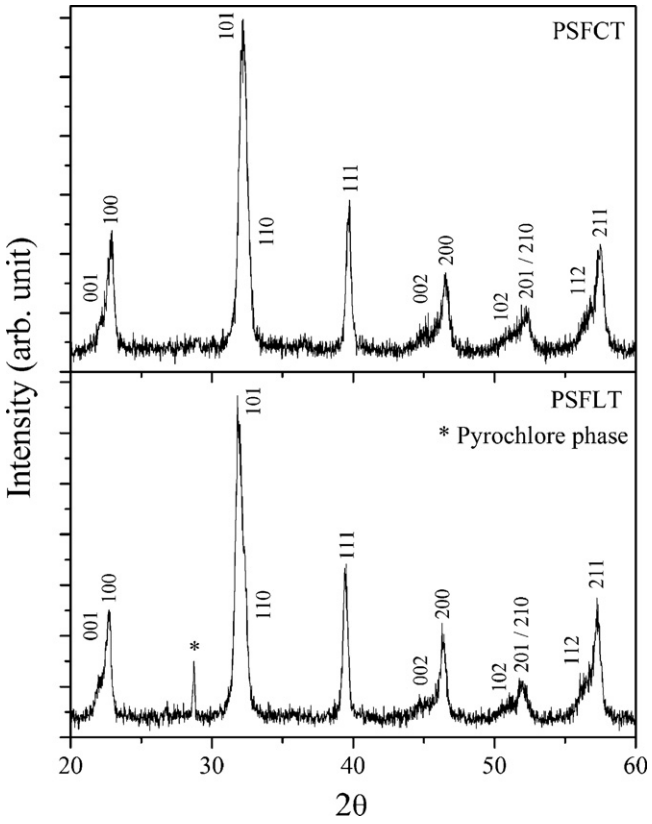

Fig. 1. XRD pattern of PSFCT and PSFLT nanoparticles heated at 700 °C/2 h.

respectively, for PSFCT and PSFLT specimens. The X-ray density is slightly higher than the apparent density. This is due to the existence of small pores in the specimens, which depends upon the sintering conditions. The calculated values of porosity are 1.4% for PSFCT and 2.4% for PSFLT pellet specimens. Fig. 2 shows the microstructures of PSFCT and PSFLT by TEM measurements and the inset is the SEM of the respective specimens. They exhibit cubic shape with slight distortion in particles as shown in the TEM image. The average particle sizes are 10 nm by TEM and 9 nm by SEM for PSFCT, and is 11 nm by TEM and 12 nm by SEM for PSFLT nanoparticles. These values of particles size from TEM/SEM images are consistent with those calculated by the Scherer's relation of XRD peaks.

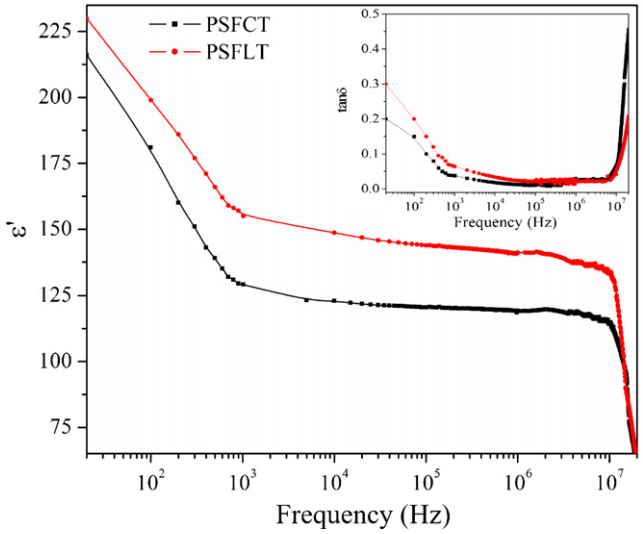

Fig. 3. Frequency dependent relative permittivity (ε') and tan δ (inset) of PSFCT and PSFLT specimens.

3.2. Dielectric properties

Fig. 3 shows the variation of relative permittivity (ε') and loss factor (tan δ) (inset) of nano MF PSFCT and PSFLT specimens with frequency 20 Hz to 20 MHz at room temperature. It can be observed that both of the specimens exhibit dielectric dispersion where ε' and tan δ decrease rapidly with increasing frequency in low-frequency region. A slight dispersion in high frequency region can be observed which varies abruptly after 15 MHz. The dielectric dispersion curve can be explained on the basis of Koop's theory [16], based on the Maxwell–Wagner model for the inhomogeneous double structure [17]. According to this model the dielectric structure was supposed to be composed of the double layer. The first layer is of fairly well conducting materials (grains), which are separated by the second thin layer (grain boundaries) of relatively poor conducting substance. The grain boundaries were found to be more

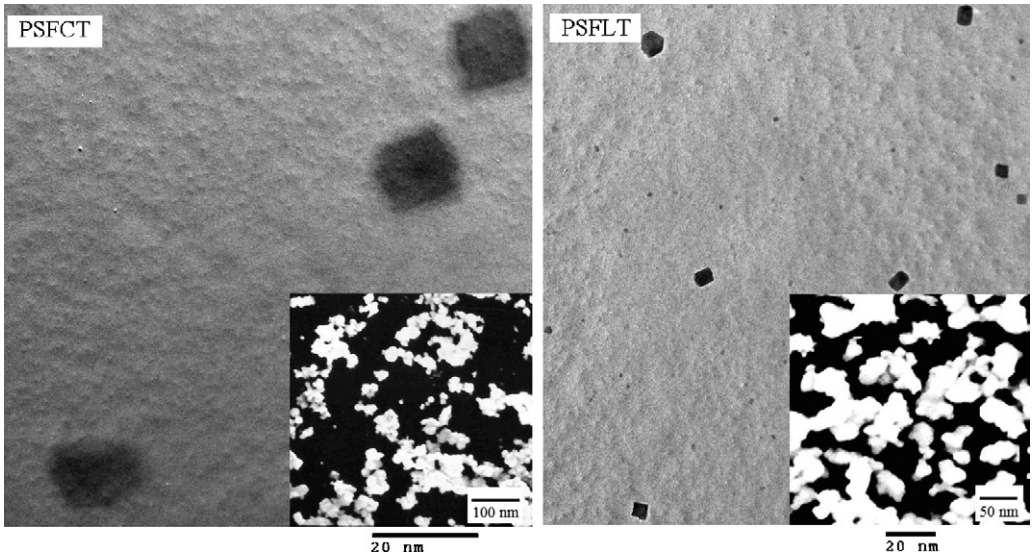

Fig. 2. TEM (inset SEM) of PSFCT and PSFLT nanoparticles.

effective at lower frequencies while the grains are more effective at higher frequency region; this will be studied in the Cole–Cole plot of IS as shown in Fig. 5. However, in an ultrafine regime, both grain boundaries and grains are large in number as compared with the bulk case, which makes the phenomena more complex. Also in nano materials, there is an additional chance of having a small dielectric constant because of large grain boundaries owing to the large *dc* resistivity. In a low-frequency regime, *dc* resistivity plays a dominant role than electronic or ionic polarization in determining the dielectric properties of MF materials [17]. In our measurements, the values of ε' are 181 and 119 with tan δ 0.15 and 0.026, respectively, at 100 Hz and 1 MHz for PSFCT specimen. However, the values of ε' are 199 and 141 with tan δ 0.22 and 0.021, respectively, observed at 100 Hz and 1 MHz for PSFLT. The observed decrease in dielectric constant with increasing frequency is attributed to the fact that the space charge carriers in a dielectric require a finite time to line up their axes in the direction of an applied alternating field. If the frequency of the field reversal increases, a point reaches when the space charge carriers cannot align with the applied field and does not follow the alternation of the field [18]; as a result dielectric constant of the material decreases. As the frequency of the field continues to increase, at some stage, the space charge polarization will barely have started to move before the field reverses and makes virtually no contribution to the polarization and hence to the dielectric constant of the material. However, in the middle of frequency region, a slight variation in ε' is observed. Such variation in ε' is explained on the basis of Stoner–Wohlfarth model [19] concerning randomly distributed single domain particles without interaction and the present magnetic nanograins are elongated towards the grain boundaries and shows dynamic behavior of ε'. The large value of dielectric constant at lower frequency is due to the predominance of species like Pb^{2+} vacancies, Fe^{2+} ions, oxygen vacancies, grain boundary defects, space charge by electrode, etc. Also, PSFLT specimen shows higher value of ε' with low loss which may be due to slightly large grain size which contributes lesser value of *dc* resistivity [2] and occurrence of pyrochlore phase than PSFCT. The dielectric loss gives value of the loss of energy from the applied field into the specimen. This is caused by domain wall resonance. At higher frequencies the losses are found to be low, since domain wall motion is inhibited and magnetization is forced to change rotation. After 15 MHz the abrupt variation in ε' and tan δ may occur due to resonance effect [9].

3.3. Impedance measurements

Fig. 4 shows the variation of the real part of impedance (Z') with frequency at various temperatures for both PSFCT and PSFLT specimens. It is observed that the magnitude of Z' decreases with increase in both frequency and temperature, indicating an increase in *ac* conductivity with rise in temperature and frequency. The Z' values for all temperatures merge at high frequency. This may be attributed to the increase of *ac* conductivity with temperature and frequency in the higher frequency region due to the removal of space charge as a result of reduction in barrier height [20]. This may be a responsible factor for the enhancement of *ac* conductivity of the material with temperature at high frequencies. Further, at low frequency, Z' values decrease with an increase in temperature and show negative temperature coefficient of resistance (NTCR) type behavior similar to that of semiconductors. The variation of imaginary part, Z'' with frequency and temperature [insets of Fig. 4] shows important features of loss spectrum mechanism. As the temperature increases, the peaks are more and more obviously in these specimens indicating relaxation is stronger at higher temperatures. It can be seen that the curves display broad and low intensity peaks with asymmetrical shape. The broadening of the peak and half widths of the peaks indicate multiple relaxations and deviations from Debye behavior [11]. This is an indication of loss in the materials which is higher at lower temperature.

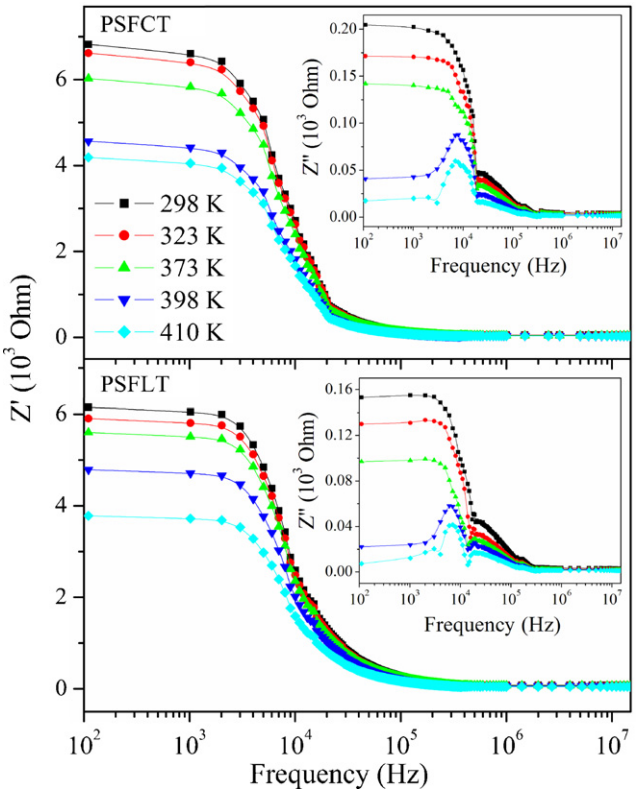

Fig. 4. The real part of impedance as a function of frequency at different temperatures.

In order to study the impedance spectrum corresponding to different effects such as grain boundaries, grains (bulk or intrinsic properties of material) and electrode contribution, Cole–Cole analysis [21] has been performed. Fig. 5 shows Cole–Cole plots (a plot drawn between imaginary (Z'') and real parts (Z') of the impedance) at various temperatures. At room temperature measurements, no semicircle formation takes place. With increasing temperature, the behavior of Z' versus Z'' transform into semicircles indicates the increase in conductivity of the materials. At 410 K, both of PSFCT and PSFLT specimens show separate arc of semicircles to the establishment of the effect of grains, grain boundary and electrodes. The center of semicircle making an angle φ with *x*-axis and is temperature-dependent reveals the non-Debye type relaxation process in the material. The appearance of three semicircles in the Cole–Cole plots at high temperatures indicates that, there are three relaxational mechanisms, which are due to grain, grain boundary and interfaces [22]. The formation of semicircular arcs in the complex impedance spectrum is governed by identifying an equivalent circuit which contains a series of array of parallel *RC* elements [22]. The low frequency semicircular arc is due to electrode interface with bulk, the middle can be assigned to the grain boundary effect, whereas the higher frequency semicircular arc can be assigned to the grain (bulk) of the material. The intercept of the semicircular arcs on the real axis (Z') gives the grain resistance (R_g) and grain boundary resistance (R_{gb}). The frequency at the maxima of semicircle, ω_{max}, for each *RC* element is given by, $\omega_{max} = 2\pi f_{max} = (RC)^{-1} = \tau^{-1}$, where the time constant, τ, f_{max} are intrinsic properties of the *RC* element, because they are independent of specimen geometry [23]. Grain and grain boundary fitting parameters (R_g, R_{gb}, τ_g and τ_{gb}) at 410 K are given in Table 1. These values indicate that the grain boundary resistance is more effective on the dielectric properties than grain contribution which is the

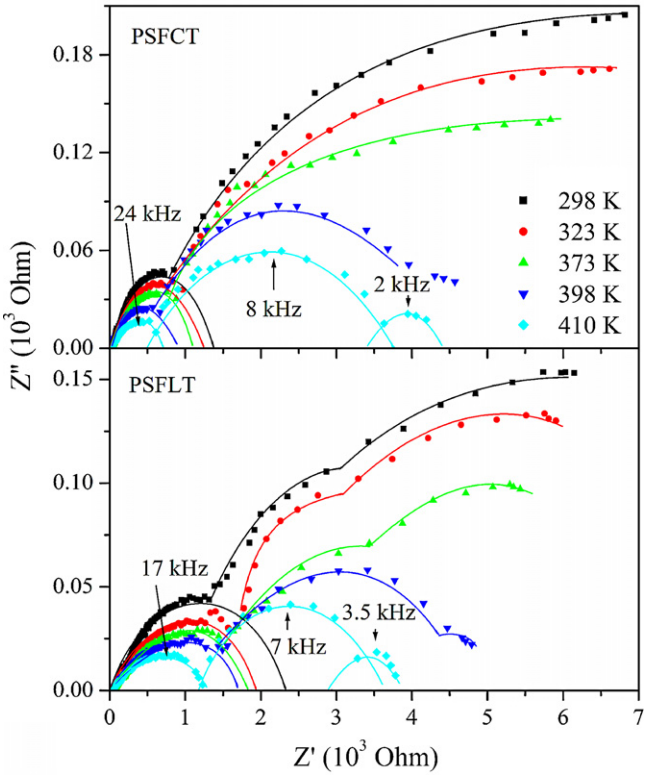

Fig. 5. The Cole–Cole plot at different temperatures.

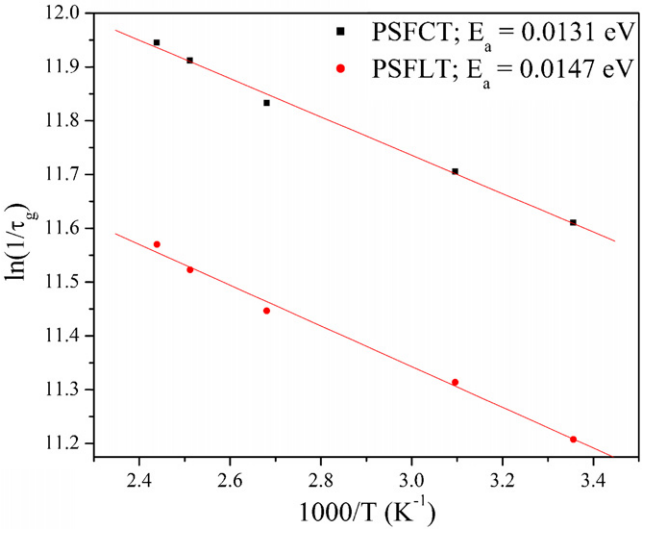

Fig. 6. Arrhenius plot for the relaxation time for grain (τ_g) with temperature.

usual behavior of nanoparticles [24]. The relaxation frequency is also higher for grain boundary which indicates the nano size effect and the occurrence of relaxor characteristics in nano structured materials.

The activation energy (E_a) of these MF materials is calculated from Arrhenius relation:

$$\tau = \tau_o \ \exp\left(\frac{-E_a}{k_B T}\right) \tag{8}$$

where τ_o is the pre exponential factor, k_B is the Boltzmann constant and T is the absolute temperature. The value of τ is taken from the arc of semicircles for grain contribution in the temperature range 298–410 K. The value of E_a calculated from the slope of $\ln(1/\tau)$ versus T^{-1} (see Fig. 6) is 0.0131 eV for PSFCT and 0.0147 eV for PSFLT nanoparticles.

Table 1
Fitting parameters obtained from impedance spectroscopy at 410 K and activation energy (E_a) from the arc of semicircles by grains.

Specimen	R_g (k)	R_{gb} (kΩ)	τ_g (10^{-6} s)	τ_{gb} (10^{-5} s)	E_a (eV)
PSFCT	0.38	1.66	6.63	1.99	0.0131
PSFLT	0.71	1.23	9.36	2.27	0.0147

4. Conclusion

The PSFCT and PSFLT nanoparticles were prepared by a chemical synthesis route using PVA as surfactant. The XRD pattern shows the coexistence of tetragonal and cubic phase in the specimens. The X-ray density (theoretical) and apparent density (experimental) have been calculated and both show small value of porosity in the specimens. The average particle size from TEM micrographs is 10 nm for PSFCT and 11 nm for PSFLT nanoparticles. At lower frequency, the dielectric properties show the normal behavior with frequency which are explained on the basis of Koop's theory and Maxwell–Wagner model. However, in the middle and higher frequency regions (10 kHz to 15 MHz) the dielectric behavior of nano size particles of the PSFCT and PSFLT specimens has been explained on the basis of Stoner–Wohlfarth model. The complex impedance measurements show three semicircles for both the specimens, which show that the resistive and capacitive properties of the specimens are associated with the grain, grain boundary and electrode. The value of resistance, $R_{gb} > R_g$, is responsible for higher frequency dependent dielectric constant. The value of activation energy is 0.0131 eV for PSFCT and 0.0147 eV for PSFLT nanoparticles.

References

[1] V.R. Palkar, S.K. Malik, Solid State Commun. 134 (2005) 783–787.
[2] K.C. Verma, M. Singh, R.K. Kotnala, N.S. Negi, Appl. Phys. Lett. 93 (2008) 072904.
[3] Y. Wang, C.M. Leung, S.W. Or, Y. Zhao, H. Luo, J. Alloys Compd. 487 (2009) 450–452.
[4] A Kumar, I. Rivera, R.S. Katiyar, J.F. Scott, Appl. Phys. Lett. 92 (2008) 132913 - 3.
[5] W. Chen, S. Shannigrahi, X.F. Chen, Z.H. Wang, W. Zhu, O.K. Tan, Solid State Commun. 150 (2010) 271–274.
[6] A.R. Chaudhuri, S.B. Krupanidhi, P. Mandal, A. Sundaresan, J. Appl. Phys. 106 (2009) 054103 - 8.
[7] K.C. Verma, R.K. Kotnala, M.C. Mathpal, N. Thakur, P. Gautam, N.S. Negi, Mater. Chem. Phys. 114 (2009) 576–579.
[8] L. Chen, W. Ren, W. Zhu, Z.G. Ye, P. Shi, X. Chen, X. Wu, X. Yao, Thin Solid Films 518 (2010) 1637–1640.
[9] K.C. Verma, R.K. Kotnala, V. Verma, N.S. Negi, Thin Solid Films 518 (2010) 3320–3325.
[10] G.T. Niitsu Gilberto, H. Nagata, A.C.M. Rodrigues, J. Appl. Phys. 95 (2004) 3116–3119.
[11] Y.M. Li, R.H. Liao, X.P. Jiang, Y.P. Zhang, J. Alloys Compd. 484 (2009) 961–965.
[12] A. Singh, V. Pandey, R.K. Kotnala, D. Pandey, Phys. Rev. Lett. 101 (2008) 247602 - 4.
[13] K.C. Verma, R.K. Kotnala, N.S. Negi, Appl. Phys. Lett. 92 (2008) 152902 - 3.
[14] K.C. Verma, M. Ram, R.K. Kotnala, S.S. Bhatt, N.S. Negi, Indian J. Pure Appl. Phys. 48 (2010) 593–599.
[15] J. Mata, A. Duran, E. Martınez, R. Escamilla, J. Heiras, J.M. Siqueiros, J. Phys.: Condens. Matter 18 (2006) 10509–10520.
[16] C.G. Koops, Phys. Rev. 83 (1951) 121.
[17] K.W. Wagner, Ann. Phys. 40 (1913) 817.
[18] V.R. Murthy, J. Sobhananadri, Phys. Stat. Sol. A 36 (1977) K133.
[19] C. Tannous, J. Gieraltowski, Eur. J. Phys. 29 (2008) 475.
[20] K. Lily, K. Kumari, R.N.P. Prasad, Choudhary, J. Alloys Compd. 453 (2008) 325.
[21] K.S. Cole, R.H. Cole, J. Chem. Phys. 9 (1941) 341.
[22] J.R. Macdonald, Impedance Spectroscopy, Wiley, NY, 1987.
[23] M.C. Steil, F. Thevenot, M. Kleitz, J. Electrochem. Soc. 144 (1997) 390.
[24] A.C. Bose, P. Thangadurai, S. Ramasamy, V. Ganesan, S. Asokan, Nanotechnology 17 (2006) 1752.